

Tidal evolution and diffusive growth during high-eccentricity planet migration: revisiting the eccentricity distribution of hot Jupiters

HANG YU ¹, NEVIN N. WEINBERG ² AND PHIL ARRAS ³

¹TAPIR, Walter Burke Institute for Theoretical Physics, Mailcode 350-17 California Institute of Technology, Pasadena, CA 91125, USA

²Department of Physics, University of Texas at Arlington, Arlington, TX 76019, USA

³Department of Astronomy, University of Virginia, P.O. Box 400325, Charlottesville, VA 22904, USA

ABSTRACT

High-eccentricity tidal migration is a potential formation channel for hot Jupiters. During this process, the planetary f-mode may experience a phase of diffusive growth, allowing its energy to quickly build up to large values. In Yu et al. (2021), we demonstrated that nonlinear mode interactions between a parent f-mode and daughter f- and p-modes expand the parameter space over which the diffusive growth of the parent is triggered. We extend that study by incorporating (1) the angular momentum transfer between the orbit and the mode, and consequently the evolution of the pericenter distance, (2) a phenomenological correction to the nonlinear frequency shift at high parent mode energies, and (3) dissipation of the parent’s energy due to both turbulent convective damping of the daughter modes and strongly nonlinear wave-breaking events. The new ingredients allow us to follow the coupled evolution of the mode and orbit over $\gtrsim 10^4$ years, covering the diffusive evolution from its onset to its termination. We find that the semi-major axis shrinks by a factor of nearly ten over 10^4 years, corresponding to a tidal quality factor $\mathcal{Q} \sim 10$. The f-mode’s diffusive growth terminates while the eccentricity is still high, at around $e = 0.8 - 0.95$. Using these results, we revisit the eccentricity distribution of proto-hot Jupiters. We estimate that less than 1 proto-HJ with eccentricity > 0.9 should be expected in *Kepler*’s data once the diffusive regime is accounted for, explaining the observed paucity of this population.

Keywords: Exoplanets (498) — Hot Jupiters (753) — Exoplanet tides (497) — Exoplanet migration (2205) — Hydrodynamics (1963)

1. INTRODUCTION

In the standard scenario, tidal friction in a binary system arises when the motions induced by a time-changing tidal force are damped away irreversibly to heat within the bodies. The time variation may be due to either an eccentric orbit or an asynchronous or misaligned spin as compared to the orbital angular momentum. As encapsulated by Darwin’s theory (Darwin 1879), friction causes a lag in the response of the body as compared to the driving force, and the forces from the resulting misaligned tidal bulge lead to secular exchange of energy and angular momentum between the two bodies and the orbit. Analytic formulas for the evolution of

the orbit and spins are typically parametrized with a tidal \mathcal{Q} or lag time τ (e.g., Goldreich & Soter 1966; Hut 1981), or attempts are made to calculate the dissipation from first principles.

For the case of highly eccentric orbits, Mardling (1995) suggested a qualitatively different route for tidal evolution as compared to Darwin’s theory. In Mardling (1995), the pericenter distance is assumed to be so close that the tidal “kicks” applied near pericenter can excite internal oscillation modes to significant energies. The energy transfer alters the orbit and changes its period. Importantly, these changes in orbital period may be so large that the phase of the oscillation mode at each pericenter passage is effectively random compared to the last, which will lead to a random walk in mode energy. On average, the mode amplitude (energy) grows as the square root (linearly) with the number of pericen-

ter passages. This behavior is called the “diffusive” or “chaotic” tide.

If the system is conservative, the diffusive tide allows the mode energy to build up until the coupled orbital and mode degrees of freedom reach an approximate equipartition (Mardling 1995; Vick & Lai 2018). If dissipation is involved and keeps removing energy from the mode, then on average there will be a net energy flowing continuously from the orbit to the mode. This may lead to a phase of rapid orbital evolution in which the orbital energy changes by many times its initial value and the semi-major axis decreases by factors of a few.

The diffusive tide may be an important process in the high-eccentricity migration of proto-hot Jupiters (HJs). In this formation scenario for HJs, the planet is born beyond the snow line at $\gtrsim 1$ AU, its eccentricity is driven to high values through interactions with another planet or star (see, e.g., Rasio & Ford 1996; Wu & Murray 2003; Fabrycky & Tremaine 2007; Chatterjee et al. 2008; Wu & Lithwick 2011; Teyssandier et al. 2013; Petrovich & Tremaine 2016; Muñoz et al. 2016; Hamers et al. 2017), and then strong tidal dissipation in the planet damps the eccentricity and shrinks the orbital semi-major axis. If one simply applies Darwin’s theory to this channel, it would predict a large number of proto-HJs with high orbital eccentricities (Socrates et al. 2012). The lack of observed systems in the high eccentricity state (Dawson et al. 2015) thus leads to a tension between the theory and observation, seemingly disfavoring the high-eccentricity migration channel.

Nevertheless, the tension could be naturally reconciled with the incorporation of the diffusive tide, as demonstrated in a number of studies (Ivanov & Papaloizou 2004, 2007; Wu 2018; Vick & Lai 2018; Vick et al. 2019). In particular, Wu (2018) showed that the $l = 2$ f-mode of the planet can grow rapidly to very significant energies. If this energy can be further dissipated somehow via nonlinear processes, it can then lead to rapid orbital evolution on $\sim 10^4$ yr timescales. This would correspond to a tidal quality factor $Q \sim 1 - 10$, which is about four to five orders of magnitude smaller than Jupiter’s. Wu (2018) showed that this could explain the paucity of highly eccentric systems found by *Kepler* because the circularization is so fast during the high-eccentricity phase that catching one in this state is observationally unlikely.

Previous studies considered the diffusive tide in the linear approximation. In this approach, the source of randomness of the f-mode phase is tidal back-reaction on the orbit. In our previous work (Yu et al. 2021), we extended the analysis by including weakly nonlinear mode interactions between the parent f-mode (the

mode that couples directly to the tide) and daughter f- and p-modes. We showed that the mode interactions lead to an energy-dependent shift of the parent f-mode’s oscillating frequency. As a result, they provide another channel for randomizing the f-mode’s phase, in addition to the tidal back-reaction considered by previous studies. The phase shift produced by the two channels are formally the same order in terms of the energy transfer at each pericenter passage and therefore have comparable significance in triggering the diffusive tide. However, once typical parameters of a proto-HJ are plugged in, we showed in Yu et al. (2021) that the phase shift due to nonlinear mode interactions is ≈ 5 times greater than that due to tidal back-reaction on the orbit. Therefore, it is nonlinear interactions that dominate the triggering and subsequent maintenance of the diffusive tidal evolution in migrating proto-HJs.

In Yu et al. (2021), we only considered the parameter space that can trigger the diffusive tide. We extend the study here by now considering the long-term evolution of the system over $\sim 10^4$ yr. In Section 3, we describe the formalism and extensions to Yu et al. (2021) that allow us to solve for the long term evolution. In Section 4 we present the results of evolving the coupled mode and orbit equations over $\sim 10^4$ yr including nonlinear mode interactions. But first, in Section 2, we show the impact of the diffusive tide on the expected number density of migrating proto-HJs and compare the results with the observed population.

2. ECCENTRICITY DISTRIBUTION OF MIGRATING PROTO-HOT JUPITERS

A key result of our study is the influence of the diffusive tide on the eccentricity distribution of migrating proto-HJs. To evaluate this, we follow the prescription outlined in Socrates et al. (2012) but generalize the treatment to allow two phases of orbital evolution. During the initial phase, when the diffusive tide operates, the orbital energy is efficiently removed and the orbital evolution is fast. Later, when the diffusive growth terminates (whose condition we will explore in later sections), the orbital evolution slows considerably.

Quantitatively, we assume there is a constant current of migrating planets, and therefore

$$\frac{dN(e; L)}{de} \frac{de}{dt} = \text{const.}, \quad (1)$$

where $N(e; L)$ is the total number of planets with orbital eccentricity less than e and orbital angular momentum (AM) $\simeq L$. We assume the planet migrates along a track of constant L , which is a good approximation since the transfer of orbital AM into the planetary f-mode by the

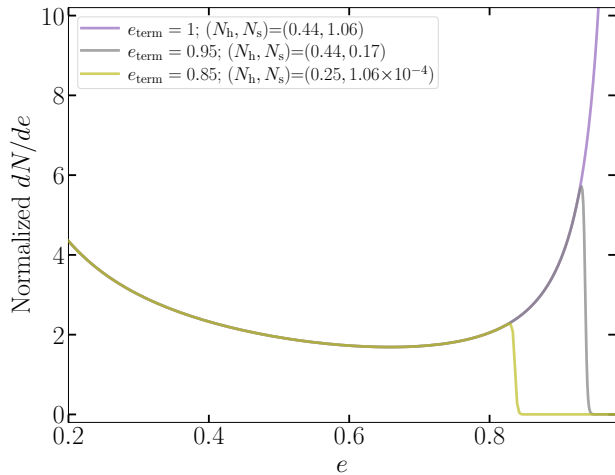


Figure 1. Number density as a function of the orbital eccentricity of migrating proto-hot Jupiters. We show in the legend the number of highly-eccentric (denoted by N_h ; corresponding to $0.7 < e < 0.9$) or super-eccentric (denoted by N_s , $0.9 < e < e_{\max}$) systems relative to mildly-eccentric systems (denoted by N_m ; corresponding to $0.2 < e < 0.6$). Line colors indicate different assumptions about the eccentricity e_{term} at which diffusive growth terminates with purple, gray, and olive lines corresponding to $e_{\text{term}} = (1, 0.95, 0.85)$, respectively.

diffusive tide changes L by less than 1% (see Sections 3.1 and 4.1). At any time, the number density of migrating planets with angular momentum L at eccentricity e is therefore given by $dN/de \propto 1/|de/dt|$. To calculate de/dt , we follow the phenomenological approach of Hut (1981) and assume the planet is pseudo-synchronized, which implies¹

$$\frac{de}{dt} = -\frac{1}{2T(e)}e(1-e^2)^{3/2}g(e), \quad (2)$$

where

$$g(e) = \frac{7 + \frac{45}{2}e^2 + 56e^4 + \frac{685}{32}e^6 + \frac{255}{64}e^8 + \frac{25}{256}e^{10}}{3(1 + 3e^2 + \frac{3}{8}e^4)}, \quad (3)$$

¹ Two caveats exist when adopting the model by Hut (1981). The first is that after the diffusive tide terminates, we still approximate the tidal lag time as a constant. This is not necessarily a good assumption as the tidal lag time is not a fundamental property of the planet and it can depend sensitively on the driving frequency (see, e.g., Ogilvie & Lin 2004; Weinberg et al. 2012). In fact, what drives the evolution from $e \sim 0.8$ to nearly zero eccentricity remains unclear. The second is that we set the rotation rate according to the pseudo-synchronization value. This may be inaccurate during the diffusive evolution because of the AM transferred to the f-mode. While it is small compared to L , it can nonetheless be significant for the planet. Evaluating the importance of both caveats is left for future study.

and

$$T(e) = \frac{Ma^8(1-e^2)^8}{9k_2GM_*(M+M_*)R^5\tau(e)} = \frac{(M+M_*)^7L^{16}}{9k_2G^9M^{15}M_*^{17}R^5\tau(e)}. \quad (4)$$

Here M_* , a , M , R , and k_2 are, respectively, the mass of the host star, the orbital semi-major axis, and the mass, radius, and Love number of the planet. We approximate the orbital evolution as a two-phase process by letting the tidal time lag be a step function,

$$\tau(e) = \begin{cases} 0.1 \text{ s} & \text{for } e \leq e_{\text{term}}, \\ 10^3 \text{ s} & \text{for } e > e_{\text{term}}, \end{cases} \quad (5)$$

where the diffusive evolution terminates at e_{term} . Since large τ implies large $|de/dt|$, the tidal dissipation is four orders of magnitude more efficient when $e > e_{\text{term}}$ and the diffusive tide operates. By changing the value of e_{term} , we can further examine how the terminal eccentricity affects the eccentricity distribution of migrating planets. The values of e_{term} and $\tau(e)$ when $e > e_{\text{term}}$ will be justified in later sections. For $e < e_{\text{term}}$, we set $\tau = 0.1 \text{ s}$, which is motivated by the empirically measured dissipation in the Jupiter-Io system (see, e.g., Vick et al. 2019).

In Figure 1 we examine three cases. In the purple curve, we set $e_{\text{term}} = 1$, which corresponds to the case without the diffusive tide; it reduces to the scenario considered in Socrates et al. (2012). The gray and olive curves include the diffusive tide when $e > e_{\text{term}}$, with the former having $e_{\text{term}} = 0.95$ and the later having $e_{\text{term}} = 0.85$. As we will see later in Section 4, they correspond to the typical termination point of the diffusive tidal evolution under the linear theory and including nonlinear mode interactions, respectively.

Given the number density dN/de , we can further compute the number of systems in a given range of eccentricities (e_1, e_2) by computing $\int_{e_1}^{e_2} [dN(e)/de] de$. Specifically, we define systems with $0.2 < e < 0.6$ as mildly-eccentric and denote the number of such systems as N_m . As suggested in Socrates et al. (2012) (see also Dawson et al. 2015), we can use this population to calibrate various constants entering the calculation and use it to predict the number of planets at different eccentricities. We are particularly interested in N_h , the number of highly-eccentric proto-HJs (defined as $0.7 < e < 0.9$), as well as N_s the number of super-eccentric systems ($0.9 < e < e_{\max}$). Here e_{\max} is the maximum eccentricity to which a survey is sensitive. We consider in this study the number of proto-HJs in *Kepler's* data (Burke et al. 2014) and determine e_{\max} following Dawson et al.

(2015),

$$e_{\max} = \left\{ 1 - \left[\frac{(n_{\text{trans}} - 1)P_{\text{orb}}^{(f)}}{t_{\text{survey}}} \right]^{2/3} \right\}^{1/2}, \quad (6)$$

where n_{trans} is the minimum number of transits required for detection, t_{survey} is the duration of the mission, and $P_{\text{orb}}^{(f)}$ is the final (when $e = 0$) orbital period. The expression for e_{\max} follows by noting that for constant AM, $P_{\text{orb}}(1 - e^2)^{3/2} = P_{\text{orb}}^{(f)}$, and then using the fact that the maximum orbital period for which a survey can detect at least n_{trans} transits in a time t_{survey} is $P_{\text{orb}} = t_{\text{survey}}/(n_{\text{trans}} - 1)$. As in Dawson et al. (2015), we use $n_{\text{trans}} = 3$ and $t_{\text{survey}} = 4\text{yr}$ in our calculation. Note here we consider only the *intrinsic* population and do not include selection effects other than the cut in e_{\max} . In the plot, we set the normalization such that $N_{\text{m}} = 1$ and the value of $(N_{\text{h}}, N_{\text{s}})$ are shown in the legend for each curve. The curves are generated for $P_{\text{orb}}^{(f)} = 3\text{day}$. Changing the final orbital period only affects the value of N_{s} for the case without diffusive tide (i.e., the purple curve). For $P_{\text{orb}}^{(f)} = 5(10)\text{day}$, we have $N_{\text{s}} = 0.82(0.55)$ for the purple curve. Approximately, we have $N_{\text{s}} \propto [P_{\text{orb}}^{(f)}]^{-1/2}$. Other values depend weakly on $P_{\text{orb}}^{(f)}$.

If we ignore the diffusive tide (purple curve), we see that there should be a significant number of super-eccentric planets, as predicted by Socrates et al. (2012). Indeed, Dawson et al. (2015) estimated that, after correcting for selection effects, there should be about 1.5 (3) super-eccentric proto-HJs with $3\text{day} < P_{\text{orb}}^{(f)} < 5\text{day}$ ($5\text{day} < P_{\text{orb}}^{(f)} < 10\text{day}$) in *Kepler's* data. However, Dawson et al. (2015) found only $N_{\text{s}} = 0_{-0}^{+1}$ in the data. (figure 2 and section 3.2 in Dawson et al. 2015). On the other hand, including the diffusive tide can reduce this number by a significant factor. Comparing the gray curve to the purple one, we find that the number of super-eccentric proto-HJs is reduced by a factor of 6, 5, 3 for $P_{\text{orb}}^{(f)} = 3, 5, 10\text{day}$ if $e_{\text{term}} = 0.95$. If the diffusive tide could be maintained to an eccentricity $e_{\text{term}} = 0.85$ as shown in the olive curve, then it should be reduced by a factor of $\sim 10^4$. These estimates are consistent with those of Wu (2018), who considered the linear diffusive tide. The influence of the diffusive tide can therefore naturally explain the paucity of super-eccentric proto-HJs.

In order to further constrain the details of tidal migration and distinguish between, e.g., the gray and olive curves, this would require detecting a population of highly-eccentric proto-HJs with $0.7 < e < 0.9$. Assuming the gray curve (with $e_{\text{term}} = 0.95$) corresponds to

the true population, we estimate that about 10 highly-eccentric systems would be needed in order for the statistical uncertainty $\sim \sqrt{10}$ to be smaller than the difference between the gray and the olive curves. Current observations do not constrain this band well (Dawson et al. 2015) and future surveys are needed. Alternatively, a detection of a proto-HJ with $e \simeq 0.9$ and a pericenter distance sufficiently small to trigger diffusion during its evolution (Wu 2018; Yu et al. 2021) could also distinguish the gray and the olive curves.²

3. FORMALISM FOR THE DYNAMICAL TIDE

In the previous section we, illustrated the key observational consequence of the diffusive tide, i.e., explaining the observed paucity of super-eccentric proto-HJs. In this section, we first review the key ingredients needed to construct an iterative mapping to evolve the tidal amplitude equation, following the framework outlined in Yu et al. (2021) (see also Ivanov & Papaloizou 2004; Wu 2018; Vick & Lai 2018; Vick et al. 2019). We then describe additional physics not accounted for in our original analysis, including orbital AM transfer, higher order corrections to the frequency shift, and strongly nonlinear energy dissipation (Sections 3.1, 3.2, and 3.3, respectively).

Suppose the host star (of mass M_*) raises a tide in the planet (of mass M) with a Lagrangian displacement $\xi(\mathbf{x}, t)$. We can expand $\xi(\mathbf{x}, t)$ as (Schenk et al. 2002; Weinberg et al. 2012)

$$\begin{cases} \xi(\mathbf{x}, t) = \sum_a q_a(t)\xi_a(\mathbf{x}, t) \\ \dot{\xi}(\mathbf{x}, t) = \sum_a (-i\omega_a)q_a(t)\xi_a(\mathbf{x}, t), \end{cases} \quad (7)$$

where $q_a(t)$ is the amplitude of an eigenmode and ω_a is its eigenfrequency. The sums run over both radial and angular quantum numbers as well as modes with both positive and negative frequencies. We normalize each mode such that

$$2\omega_a^2 \int d^3x \rho \xi_{a'}^* \cdot \xi_a = E_0 \delta_{aa'}, \quad (8)$$

where $E_0 = GM^2/R$. For a parent mode that directly couples to the tide, its evolution in the co-rotating frame

² We note that HD 80606b has an eccentricity of $e = 0.983$ (Wu & Murray 2003). However, its pericenter distance is too large to trigger diffusive growth given its radius of $\simeq 0.9R_J$. See also the discussion in Wu (2018). This suggests that the number density of proto-HJs is in fact more complicated than the framework proposed in Socrates et al. (2012) which we adopt here. Instead, the properties of the planet itself, such as its radius, could also play crucial roles (see discussions in Appendix A). Further investigations are thus required.

is described by the amplitude equation (Yu et al. 2021)

$$\dot{q}_a + [i(\omega_a + \delta\omega_a) + (\gamma_a + \delta\gamma_a)] q_a = i\omega_a U_a, \quad (9)$$

where the linear tidal forcing is given by

$$U_a(t) = W_{lm} Q_a \left(\frac{M_*}{M} \right) \left[\frac{R}{D(t)} \right]^{l+1} \exp \{ -im [\Phi(t) - \Omega_s t] \}, \quad (10)$$

where D is the orbital separation, Φ is the orbital phase, Ω_s is the spin of the planet, the linear tidal overlap $Q_a = (MR^l)^{-1} \int d^3 r \rho \xi^* \cdot \nabla (r^l Y_{lm})$, and at leading order ($l = 2$), the nonvanishing W_{lm} coefficients are $W_{2\pm 2} = \sqrt{3\pi/10}$ and $W_{20} = -\sqrt{\pi/5}$. The quantities ω_a and γ_a are the linear eigenfrequency and damping rate of the mode, and $\delta\omega_a$ and $\delta\gamma_a$ are the nonlinear corrections caused by the parent mode (an $l_a = 2$ f-mode) interacting with high-order daughter f- and p-modes (Yu et al. 2021). For small mode energy $\tilde{E}_a \equiv |q_a|^2 (< |\omega_a/\Omega| < 1)$, the nonlinear corrections can be expressed as (Yu et al. 2021)

$$\delta\omega_a = \Omega \tilde{E}_a, \quad (11)$$

$$\delta\gamma_a = \Gamma \tilde{E}_a, \quad (12)$$

where Ω and $\Gamma \propto \omega_a$ are constants determined by the internal structure of the planet. The typical values of Ω and Γ will be presented later in Table 1. Here, as in Yu et al. (2021), we use the tilde symbol to indicate energy normalized by E_0 . For instance, $\tilde{E}_{\text{orb},k} = E_{\text{orb},k}/E_0$.

Upon a Doppler frequency shift (and ignoring other rotational corrections for simplicity), we can also transfer the co-rotating frame mode amplitude equation (Equation (9)) to the inertial frame,

$$\dot{q}'_a + [i(\omega'_a + \delta\omega_a) + (\gamma_a + \delta\gamma_a)] q'_a = i\omega_a U'_a, \quad (13)$$

where $q'_a = q_a \exp(-im_a \Omega_s t)$, $\omega'_a = \omega_a + m_a \Omega_s$, and $U'_a = U_a \exp(-im_a \Omega_s t)$.

When the orbit is highly eccentric and the tidal interaction is only significant near each pericenter passage, Equation (13) can be evolved together with the orbit via a set of iterative mapping equations (assuming weak damping; the more general form will be presented in Section 3.2)

$$q'_{a,k(0)} = q'_{a,k-1(1)} + \Delta q_{a,k} \quad (14)$$

$$q'_{a,k(1)} = q'_{a,k(0)} e^{-[i(\omega'_a + \Omega \tilde{E}_{a,k(0)}) + (\gamma_a + \Gamma \tilde{E}_{a,k(0)})] P_{\text{orb},k}}, \quad (15)$$

$$\tilde{E}_{\text{orb},k} - \tilde{E}_{\text{orb},k-1} = -(\tilde{E}_{a,k(0)} - \tilde{E}_{a,k-1(1)}) = -\Delta \tilde{E}_{a,k}, \quad (16)$$

$$\frac{P_{\text{orb},k}}{P_{\text{orb},k-1}} = \left(\frac{\tilde{E}_{\text{orb},k}}{\tilde{E}_{\text{orb},k-1}} \right)^{-3/2}, \quad (17)$$

where the superscript (0) and (1) indicate that the amplitudes are, respectively, evaluated right after and

right before a pericenter passage. We have also defined $\tilde{E}_{a,k(0)} = |q'_{a,k(0)}|^2$ and similarly for $\tilde{E}_{a,k-1(1)}$. The tidal interaction at each pericenter is characterized by a kick in the mode amplitude, $\Delta q_{a,k}$, given by

$$\begin{aligned} \Delta q_{a,k} &= \int i\omega_a U'_a(t) e^{i(\omega'_a + \gamma_a)t} dt, \\ &= i2\pi Q_a K_{lm}(\omega'_a, \Omega_{\text{peri}}) \\ &\quad \times \left(\frac{\omega_a \Omega_{\text{peri}}^2}{\omega_0^3} \right) \left(\frac{M_*}{M + M_*} \right) \left(\frac{R}{D_{\text{peri}}} \right)^{l-2}, \end{aligned} \quad (18)$$

where $D_{\text{peri}} \equiv a(1 - e)$ is the pericenter distance, $\Omega_{\text{peri}}^2 \equiv G(M + M_*)/D_{\text{peri}}^3$, and $\omega_0^2 = GM/R^3$. The quantity K_{lm} , which corresponds to the temporal overlap between the orbit and the mode, is given by (Press & Teukolsky 1977)

$$K_{lm}(\omega, \Omega_{\text{peri}}) = \frac{\omega_0 W_{lm}}{2\pi} \int \left[\frac{D_{\text{peri}}}{D(t)} \right]^{l+1} e^{i[\omega t - m\Phi(t)]} dt. \quad (19)$$

Assuming a nearly parabolic orbit and ignoring tidal back-reaction, one can further write K_{22} (corresponding to the prograde $l = m = 2$ harmonic which dominates the tidal interaction) as (Lai 1997)

$$\begin{aligned} K_{22}(\omega, \Omega_{\text{peri}}) &\simeq \frac{2z^{3/2} e^{-2z/3}}{\sqrt{15}} \left(\frac{\omega_0}{\Omega_{\text{peri}}} \right) \left(1 - \frac{\sqrt{\pi}}{4\sqrt{z}} \right), \\ &\simeq 1.1 \times 10^{-2} \left(\frac{z}{11} \right)^{-5.7} \left(\frac{\omega_0}{\Omega_{\text{peri}}} \right), \end{aligned} \quad (20)$$

where $z \equiv \sqrt{2}\omega/\Omega_{\text{peri}}$. Note that in the second equality we have expanded the expression around $z = 11$, which is a typical value for systems we consider in this study.

For future convenience, we define the one-kick energy as

$$\Delta \tilde{E}_1 \equiv |\Delta q_1|^2, \quad (21)$$

which is the energy gained by the mode after the first pericenter passage (assuming the mode starts from zero energy). Note, however, that in the subsequent passages, the mode energy gain $\Delta \tilde{E}_{a,k} \neq |\Delta q_k|^2$. Instead, if the mode has accumulated an energy $\tilde{E}_{a,k(0)} \gg \Delta \tilde{E}_1$, then the characteristic energy exchange is given by (see, e.g., Wu 2018)

$$\Delta \tilde{E}_{a,k} \sim |q'_{a,k(0)} \Delta q_{a,k}| \sim \sqrt{\tilde{E}_{a,k(0)} \Delta \tilde{E}_1}. \quad (22)$$

Here we approximated $\Delta q_k \simeq \Delta q_1 = \text{constant}$. This is because the change in D_{peri} is small and it can therefore be approximated as constant throughout the evolution (see, however, Section 3.1). Equations (18) and (20) then imply that the kick amplitude is also approximately constant.

Equations (14)-(17) provide a complete set of equations needed to evolve the system including leading-order nonlinear interactions. However, one should keep in mind that they have some potentially important limitations. Although D_{peri} is nearly constant for much of the planet’s orbital evolution, the kick Δq_k is especially sensitive to D_{peri} (Equation (20)). Furthermore, the leading-order nonlinear correction to the frequency, Equation (11), is only accurate for small parent energies. As the mode grows diffusively, it can reach $\tilde{E}_a \gtrsim |\omega_a/\Omega|$, and the frequency correction $\delta\omega_a \gtrsim \omega_a$, which is likely unphysical. As \tilde{E}_a grows even further to $\tilde{E}_a \gtrsim 0.1$, the parent mode’s displacement at the surface may reach a value $\simeq R$, and it may break due to strongly nonlinear processes (Wu 2018).

In Yu et al. (2021), we restricted the analysis to the initial phase of the evolution (the first few hundred years), when the issues noted above are not yet critical. Since we are now interested in following the system over a longer timescale ($\gtrsim 10^3$ years), we must account for them. We describe our procedure for doing so in Sections 3.1-3.3.

3.1. Orbital AM transfer

In Yu et al. (2021) and other studies (e.g., Vick & Lai 2018), the pericenter distance D_{peri} is kept constant during the evolution. This approximation is reasonable at early times because at each pericenter passage, the fractional AM transfer is much smaller than the fractional energy transfer (Appendix B) and during the highly eccentric stage, $\Delta D_{\text{peri}}/D_{\text{peri}} \simeq 2(\Delta L/L)$ since $L \simeq \mu\sqrt{2G(M+M_*)}D_{\text{peri}}$, where $\mu = MM_*/(M+M_*)$ is the reduced mass. However, the strength of the tidal kick is very sensitive to the pericenter distance (Equation (20); see also Wu 2018). We thus relax here the approximation that the pericenter distance is constant, and instead incorporate its evolution into the iterative mapping.

Together with the energy transfer from the orbit to the planet $\Delta E_{a,k} = (\tilde{E}_{a,k}^{(0)} - \tilde{E}_{a,k-1}^{(1)})E_0$, we also have an associated AM transfer $\Delta J_{a,k}$ given by (see Appendix B)

$$\Delta J_{a,k} = L_k - L_{k-1} = \frac{m_a}{\omega_a} \Delta E_a. \quad (23)$$

We use J_a to denote the AM of mode a in order to distinguish it from the orbital AM L . From the new orbital AM (together with $E_{\text{orb},k}$ or, equivalently, a_k), we can then calculate the new orbital eccentricity as

$$e_k = \left[1 - \frac{L_k^2}{\mu^2 G(M+M_*) a_k} \right]^{1/2}, \quad (24)$$

and the new pericenter distance as

$$D_{\text{peri},k} = \frac{a_k}{1 - e_k} = \frac{L_k^2}{\mu^2 G(M+M_*)(1+e_k)}. \quad (25)$$

We then update the kick amplitude in the next [($k+1$)’th] pericenter passage with the newly computed $D_{\text{peri},k}$.³

Note that we have effectively treated the planetary f-mode as a reservoir of the AM here. For simplicity, we do not consider in this study how the AM in the f-mode might be further deposited into the background planet as the mode energy is dissipated (either by strongly or weakly nonlinear processes). As a result, we do not change the spin of the background planet during the evolution. Furthermore, we ignore any AM transfer due to the equilibrium tide as the linear damping rate γ_a is extremely small and hence the torque due to the equilibrium tide is very weak. As a caveat, we note that the spin evolution of the planet could nonetheless have significant impact on the evolution of the orbit because the kick at each pericenter passage depends sensitively on the mode’s inertial-frame frequency (Equations (18) and (20)). See Section 5 and Appendix D for further discussions.

3.2. Nonlinear frequency shift

In Yu et al. (2021), we showed that the leading-order nonlinear phase shift can be described by Equation (11). It is accurate for small \tilde{E}_a yet becomes problematic when $\tilde{E}_a \simeq |\omega_a/\Omega|$, as the nonlinear frequency shift can then become greater than the linear frequency, which is unrealistic. Note that $(|\omega_a/\Omega|) < \tilde{E}_{\text{wb}}$, where $\tilde{E}_{\text{wb}} \sim 0.1$ is the wave-breaking energy of the mode (the subscript “wb” stands for wave-breaking; see Section 3.3). In other words, Equation (11) becomes inaccurate before the mode breaks by strongly nonlinear effects. In order to account for this, we adopt a phenomenological correction to the nonlinear frequency shift

$$\frac{\delta\omega_a}{\omega_a} = \frac{(\Omega/\omega_a)\tilde{E}_a}{1+x|(\Omega/\omega_a)\tilde{E}_a|}, \quad (26)$$

where $x > 0$ is left as a free parameter. For small \tilde{E}_a , this reduces to the leading-order expression derived in Yu et al. (2021). For large \tilde{E}_a , $\delta\omega/\omega_a \rightarrow \text{sign}[\Omega]/x$, and

³ In fact, the new pericenter distance should already affect the kick-amplitude at the k ’th passage and thus $\Delta E_{a,k}$. However, the fractional change in D_{peri} is only $\mathcal{O}(10^{-6})$ after a single pericenter passage; it is only the cumulative change in D_{peri} over $\mathcal{O}(10^4)$ orbital cycles that plays a mildly important role. Therefore, shifting D_{peri} by a single cycle in our mapping procedure does not affect the qualitative results.

by choosing $x > 1$ we prevent the nonlinear frequency shift from exceeding the original linear frequency.

Note that the nonlinear frequency shift $\delta\omega_a$ is a function of the mode energy \tilde{E}_a , which decays with time between pericenter passages as (see Yu et al. 2021)

$$\tilde{E}_a(t) \simeq \frac{\tilde{E}_a^{(0)}}{1 + 2 \left[\gamma_a + \Gamma \tilde{E}_a^{(0)} \right] t} \quad (27)$$

(we still approximate $\delta\gamma_a = \Gamma \tilde{E}_a$ for the dissipation and ignore further corrections to it for simplicity). To account for this, we solve the nonlinear phase as a function of the mode energy \tilde{E}_a

$$\begin{aligned} \delta\phi_{\text{nl}} &= - \int_{t_0}^t \delta\omega_a dt = - \int_{\tilde{E}_a^{(0)}}^{\tilde{E}_a} \frac{\delta\omega}{d\tilde{E}_a/dt} d\tilde{E}_a \\ &= \frac{\Omega}{2(\Gamma - x\gamma|\Omega|/\omega_a)} \\ &\quad \times \log \left\{ \left[\frac{\gamma + \Gamma \tilde{E}_a}{\gamma + \Gamma \tilde{E}_a^{(0)}} \right] \left[\frac{\omega + x|\Omega|\tilde{E}_a^{(0)}}{\omega + x|\Omega|\tilde{E}_a} \right] \right\}. \quad (28) \end{aligned}$$

Note when $x \rightarrow 0$, the above equation reduces to equation (41) in Yu et al. (2021).

Consequently, the general form (without assuming the energy dissipation is negligible) to evolve the mode when the planet is away from pericenter is given as follows (cf. Equation (15)). We first evaluate the magnitude from $|q'_{a,k}|$ to $|q'_{a,k}|^{(1)}$ using Equation (27). The phase evolution is then given by $\angle q'_{a,k}^{(1)} = \angle q'_{a,k}^{(0)} + \phi_k$, where $\phi_k = -\omega'_a P_{\text{orb},k} + \delta\phi_{\text{nl}}$ with $\delta\phi_{\text{nl}}$ given by Equation (28).

In addition to producing excess phase shift of the f-mode when the planet is away from pericenter, the nonlinear frequency shift may modify the kick the f-mode receives at each pericenter passage. This is because the kick depends on the temporal overlap K_{lm} which is a function of the mode frequency (Equation (20)). We account for this effect by replacing ω'_a with $\omega'_a + \delta\omega_a$ when evaluating K_{lm} in Equation (18). When the mode has built up a significant amount of energy by diffusion, we have $\tilde{E}_{a,k-1}^{(1)} \simeq \tilde{E}_{a,k}^{(0)} \gg \Delta\tilde{E}_{a,k}$. Consequently, we ignore the energy difference before and after the kick and simply use $\tilde{E}_{a,k-1}^{(1)}$ to evaluate a mean frequency shift $\delta\omega_a$. Because $\Omega/\omega_a < 0$ (see Table 1 and Yu et al. 2021), we see that including $\delta\omega_a$ makes the kick stronger than the linear case (Equation (20)). For example, for $\delta\omega_a/\omega_a = -0.1$, the new K_{22} is 80% greater than the linear value.

3.3. Wave breaking

While Equation (27) describes the damping of the f-mode due to weakly nonlinear interactions, we note that

such dissipation may not be sufficient to balance out the energy gain at each pericenter passage. As a result, the mode energy may increase on average as the diffusive process continues. To prevent the f-mode from growing to an unphysically large value, we follow the prescriptions proposed in Wu (2018) (see also Vick et al. 2019) and assume an *ad hoc* strongly nonlinear dissipation mechanism in addition to Equation (27).⁴

As in Wu (2018), we set $\tilde{E}_{\text{wb}} = 0.1$ as a threshold energy for the planetary f-mode since it corresponds to the mode having a radial displacement of $\simeq R$ at the surface. If the mode's energy after a pericenter passage exceeds this energy, i.e., $\tilde{E}_{a,k}^{(0)} > \tilde{E}_{\text{wb}}$, we then assume the mode breaks through a strongly nonlinear process which removes nearly all but \tilde{E}_{resi} of the mode energy within the next orbital cycle. In other words, if a wave-breaking event happens at the k 'th passage, we set the mode energy right before the next passage, $\tilde{E}_{a,(k)}^{(1)}$, to the residual value \tilde{E}_{resi} . We leave \tilde{E}_{resi} as a free parameter to be explored. The associated nonlinear evolution phase $\delta\phi_{\text{nl}}$ is randomly chosen from $[0, 2\pi)$ as such a strongly nonlinear wave-breaking should erase any memory of the original mode phase.

At this point, we have described all the ingredients necessary to evolve the system over $\sim 10^4$ yr. In the next Section, we use them to examine the coupled evolution of the mode and the orbit.

4. COUPLED EVOLUTION OF MODE AND ORBIT

Using the formalism described in the previous section, we now solve for the evolution of orbital elements and mode energy during the tidal circularization of a proto-HJ. We consider two Jupiter-mass models whose parameters are summarized in Table 1; we refer to the models according to their radii, namely the $1.1R_J$ model and the $1.7R_J$ model. Both models are constructed using MESA (version 15140; Paxton et al. 2011, 2013, 2015, 2018, 2019) and the (linear) eigenmodes are computed using GYRE (Townsend & Teitler 2013; Townsend et al. 2018). The parameters describing the nonlinear frequency shift Ω and damping rate Γ (Equations (11) and (12)) are calculated following the prescription in Yu et al. (2021). We assume that the dissipation of each daughter mode

⁴ Note here we use the word “weakly nonlinear dissipation” to refer to the dissipation we calculate from the leading-order nonlinear interaction (i.e., the three-mode interaction) perturbatively. See Yu et al. (2021) for details. This is a first-principle calculation yet it applies only when the mode energy is not too large. In contrast, we use the word “strongly nonlinear dissipation” to stand for energy dissipation happening when the mode energy growth above the wave-breaking threshold \tilde{E}_{wb} . This is a phenomenological model.

Table 1. Properties of the two Jupiter models considered in our study. We write $E_0 = GM^2/R = E_{0,43} \times 10^{43}$ erg, $\omega_0 = \sqrt{GM/R^3} = \omega_{0,-4} \times 10^{-4}$ rad s $^{-1}$.

R	$E_{0,43}$	$\omega_{0,-4}$	ω_a	Q_a	Ω	Γ
$1.1R_J$	3.1	5.1	$1.1\omega_0$	0.39	$-31\omega_a$	$7.2 \times 10^{-10}\omega_a$
$1.7R_J$	2.0	2.7	$1.1\omega_0$	0.44	$-67\omega_a$	$1.1 \times 10^{-4}\omega_a$

is due to turbulent convective damping, which we calculate following Burkart et al. (2013) (see also Shiode et al. 2012) and then sum over modes to obtain Γ .

The $1.1R_J$ model corresponds to an evolved Jupiter with an age $\sim 10^9$ yr. This is the same model as considered in Yu et al. (2021).⁵ Note that this model has a particularly weak damping due to turbulent convection and therefore the energy is mostly dissipated via strongly nonlinear wave-breaking events as described in Section 3.3. The $1.7R_J$ model corresponds to a relatively young Jupiter with an age of $\sim 10^6$ yr. The key difference is that the younger Jupiter model has a much higher turbulent convective damping rate compared to the more evolved $1.1R_J$ model. As we shall see shortly, the high damping rate could prevent the mode from evolving into the strongly nonlinear regime (at least in the first $\sim 10^4$ yr of evolution). As a result, we do not necessarily need to invoke our rather ad hoc assumptions about energy dissipation by nonlinear wave-breaking for the $1.7R_J$ model and its evolution could be qualitatively different from that of the $1.1R_J$ model.

4.1. The $1.1R_J$ model

We start by examining evolution trajectories of the evolved (age $\sim 10^9$ yr) $1.1R_J$ model.

4.1.1. Example trajectories with fiducial parameters

A few representative examples of the orbital evolution are shown in Figure 2. Here we consider a host star with $M_* = 1 M_\odot$ and an initial orbit with semi-major axis $a_0 = 1$ AU and eccentricity $e_0 = 0.980$. The initial pericenter distance is therefore $D_{\text{peri},0} = 0.020$ AU = $3.71r_t$, where the tidal radius $r_t \equiv (M_*/M)^{1/3} R$. Assuming constant AM, the final orbital period after complete circularization is $P_{\text{orb}}^{(f)} \simeq 2.8$ day. We assume that the planet is initially non-rotating and we ignore any subsequent tidal spin-up of the background planet (as discussed in Section 3.1, but see Appendix D).

We chose the orbital parameters in order that the one kick energy $\Delta\tilde{E}_1$ only slightly exceeds the thresh-

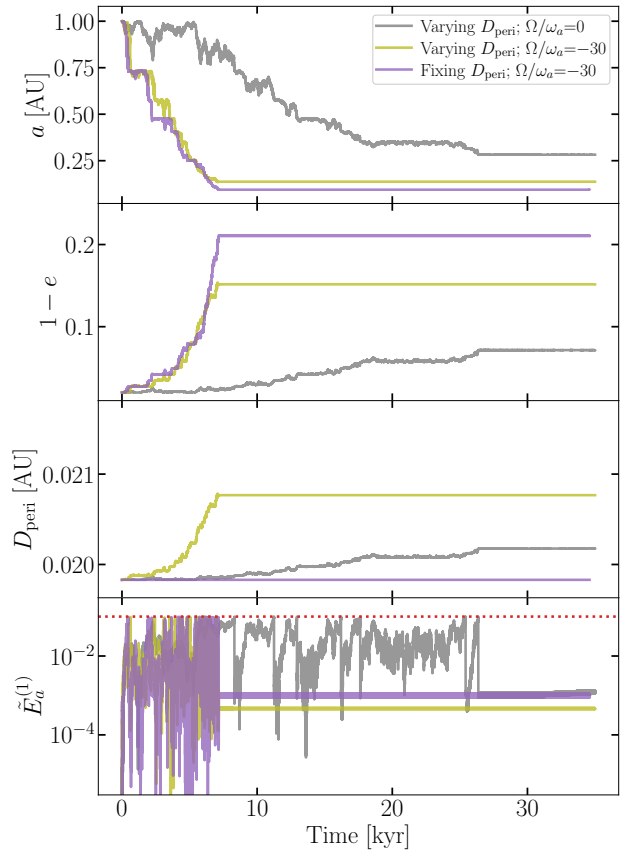


Figure 2. Evolution of the orbital elements and mode energy for the $R = 1.1R_J$ model over a duration of $\approx 3 \times 10^4$ yr. Here the one-kick energy is $\Delta\tilde{E}_1 = 1.5 \times 10^{-5}$ and the final orbital period is $P_{\text{orb}}^{(f)} = 2.8$ day. The gray curves correspond to the linear case where we ignore the nonlinear frequency shifts by setting $\Omega = 0$. The olive curves include the nonlinear frequency shift. For comparison, the purple curves show the trajectories if we prevent the pericenter distance from changing (and calculate the eccentricity using $e = (1 - D_{\text{peri}}/a)$). Because the weakly nonlinear dissipation is small in this model, the mode energy is removed via strongly nonlinear wave breaking whenever it reaches $\tilde{E}_{\text{wb}} = 0.1$, as indicated by the red-dotted line in the bottom panel. Here we assume $x = 3$ and $\tilde{E}_{\text{resi}} = 10^{-3}$.

old needed to trigger diffusion (Yu et al. 2021); its value is $\Delta\tilde{E}_1 = 1.5 \times 10^{-5}$. We selected such a $\Delta\tilde{E}_1$ for the following reason. Before the diffusive tide is triggered, one expects the eccentricity to gradually increase (and hence the pericenter distance to gradually decrease) due to, e.g., the Lidov-Kozai mechanism (Wu & Murray 2003; Fabrycky & Tremaine 2007). Once the one-kick energy increases above the threshold value, the diffusive tide quickly decouples the planet-host star system from the tertiary perturber and consequently prevents the one-kick energy from increasing further (see, e.g., Wu 2018; Vick et al. 2019).

⁵ The values of Ω and Γ presented here are slightly different from the ones in Yu et al. (2021) because different versions of MESA are used to construct the background planet model.

In Figure 2, the gray curves show the linear case in which we ignore the nonlinear frequency shift ($\Omega = 0$). For comparison, the olive curves show the nonlinear case in which the frequency shift $\Omega/\omega_a = -30$ (Table 1). We take a fiducial value of $x = 3$ in order to restrict the frequency shift at high energies (see Equation (26)). By comparing the olive and purple curves, we see the effect of allowing the pericenter distance to vary during the evolution. In particular, the olive curves show the evolution assuming the orbital AM transfer follows the prescription of Section 3.1, which then allows us to compute D_{peri} at each pericenter passage from the instantaneous orbital AM. By contrast, the purple curves assume a constant D_{peri} (as in Yu et al. 2021) and the eccentricity is computed using $e_k = 1 - (D_{\text{peri}}/a_k)$ instead of Equation (24). Note that for this model, the nonlinear damping Γ is too small to balance the energy gain. Thus we have to rely on our ad hoc wave breaking prescription to remove the mode energy (Section 3.3). Here we set $\tilde{E}_{\text{wb}} = 0.1$ as the wave-breaking threshold and $\tilde{E}_{\text{resi}} = 10^{-3}$ as the residual after each breaking event.

From Figure 2, we see that once the diffusive tide is triggered, it can reduce the orbital semi-major axis by nearly an order of magnitude over a timescale of only $\approx 10^4$ yr.

To help relate our results to observations, we can express them in terms of an effective tidal quality factor \mathcal{Q} , defined such that (Goldreich et al. 1989)

$$\frac{1}{a} \frac{da}{dt} = -\frac{21}{64} \Omega_{\text{orb}} \frac{M_*}{M} \frac{aR^5}{D_{\text{peri}}^6} \frac{k_2}{\mathcal{Q}}, \quad (29)$$

where k_2 is the tidal Love number, whose typical value is $0.3 \lesssim k_2 \lesssim 0.5$. On average, we find that the orbit decays by about 1 AU in 10^4 yr (Figure 2), which implies

$$\frac{\mathcal{Q}}{k_2} \simeq 14 \left(\frac{P_{\text{orb}}}{1 \text{ yr}} \right)^{1/3} \left(\frac{D_{\text{peri}}}{0.02 \text{ AU}} \right)^{-6} \left(\frac{|da/dt|}{1 \text{ AU}/10^4 \text{ yr}} \right)^{-1} \quad (30)$$

This is about 4 to 5 orders of magnitude smaller than the empirically determined \mathcal{Q} inferred for the Jupiter-Io system. The corresponding tidal lag time (Ogilvie 2014) is $\tau \equiv 1/(\mathcal{Q}\omega_d) \simeq 10^3$ s at a driving frequency $\omega_d = 2\pi/(1 \text{ day})$, which motivates our choice of τ in Equation (5).

It is important to note that the diffusive tide does not circularize the orbit down to zero eccentricity. Instead, in all three cases plotted in Figure 2, the evolution due to diffusive tide terminates when the eccentricity is still high. Under the linear theory (gray curves), the evolution terminates at the largest orbital eccentricity and we still have $e > 0.9$ when the diffusive evolution stalls.

Including the nonlinear frequency shift helps circularizing the orbit further, though we still have $e \sim 0.8$ when the diffusive tide terminates. Taking into account the increase in D_{peri} also hinders the circularization process compared to the case where D_{peri} is held constant.

4.1.2. Statistics of the termination point

Because the diffusive tidal evolution is a stochastic process, the termination point of a particular system, as shown in Figure 2, is sensitive to the initial conditions. Here we examine the statistics of the termination point in Figure 3 by giving the mode a small initial amplitude $|q_{a,0}| = 10^{-5}$ but a random phase. Because the evolution is chaotic (Vick & Lai 2018), varying the initial conditions allows us to obtain different trajectories for the same set of parameters. The median values of the distribution of the termination point are connected with solid lines in Figure 3, and each error bar corresponds to the 20'th and 80'th percentiles for the specific set of parameters. If a parameter is not explicitly listed in the legend, its value is that given in Figure 2.

Along the x-axis, we vary the value of the nonlinear frequency shift Ω/ω_a ; the leftmost point (with $\Omega = 0$) corresponds to the linear case. i.e., ignoring nonlinear mode interactions. Towards the right, the magnitude of the nonlinear frequency (and hence phase) shift increases, which helps prolong the diffusive tidal evolution and drive the system to smaller terminal values of a and e . Specifically, when $\Omega = 0$ and we ignore the nonlinear frequency shift, the evolution terminates at $e > 0.9$ under all the scenarios we consider in Figure 3. When we include the nonlinear frequency shift, the circularization continues down to $e \simeq 0.8 - 0.85$.

The effect of allowing the pericenter distance to vary can be seen by comparing the gray and olive curves. For the linear case, it does not typically affect the results since the evolution stalls before the pericenter can change significantly. By contrast, when the nonlinear frequency shift is incorporated, the circularization continues further and the increasing pericenter distance plays a more important role in terminating the orbital evolution and preventing the orbital eccentricity from dropping below $e \simeq 0.8$.

Another factor limiting the circularization is the value of x , introduced to avoid the nonlinear frequency shift from becoming greater than the original linear eigenfrequency (Section 3.2). Its effect can be seen by comparing the olive and purple curves. As x increases, the maximum fractional frequency shift ($\simeq 1/x$) decreases in our phenomenological model (Equation (26)). This causes the circularization to stall at greater values of e as x

increases. It also causes the plateau of both a and e for large values of $|\Omega/\omega_a|$ in Figure 3.

Lastly, we examine the effect of \tilde{E}_{resi} , the residual energy after a wave-breaking event, by comparing the olive and cyan curves. While the cyan curve has an \tilde{E}_{resi} that is 50 times greater than the one used for the olive curve, its terminal a_{orb} is only slightly smaller. Consequently, the circularization is not sensitive to the value of \tilde{E}_{resi} (to understand why, see discussions following Equations (32) and (34) below).

4.1.3. Analytic estimates

The numerical results shown in Figures 2 and 3 can be understood analytically. The key is that for the diffusive tide to remain active, the phase difference between two adjacent orbits,⁶ $\Delta\phi_k = \phi_k - \phi_{k-1}$, needs to satisfy $|\Delta\phi_k| \gtrsim 1$ rad on average (see also the discussions in Wu 2018; Vick et al. 2019; Yu et al. 2021). By evaluating $\Delta\phi_k$ as a function of, e.g., the semi-major axis of the orbit a , and then inverting the relation, we can estimate the termination point when the phase difference is no longer large enough to maintain the diffusion.

Under the linear theory, we have

$$\Delta\phi_{\text{br},k} = -\omega'_a \Delta P_{\text{orb},k} = \frac{3}{2} \omega'_a P_{\text{orb},k} \frac{\Delta\tilde{E}_k}{|\tilde{E}_{\text{orb},k}|}, \quad (31)$$

where the subscript “br” stands for back-reaction, as it is the only channel to create $\Delta\phi_k$ under the linear theory. To evaluate the energy change $\Delta\tilde{E}_k$, we use Equation (22). The evolution terminates when $|\Delta\phi_{\text{br},k}| \sim 1$ rad (but not exactly 1 rad). Since we are mostly interested in how the final a scales with different parameters, and our estimates of both $\Delta\tilde{E}_{a,k}$ and the terminal $|\Delta\phi_{\text{br},k}|$ are accurate only to order unity, we drop all the numerical prefactors and simply absorb them into an overall scaling factor λ_{br} .

Using this approach, the semi-major axis when diffusive growth terminates is given by

$$\begin{aligned} a_{\text{term}}^{(\text{br})} &\simeq 0.5 \text{ AU} \\ &\times \left(\frac{\lambda_{\text{br}}}{0.1}\right)^{2/5} \left(\frac{\Delta\tilde{E}_1}{10^{-5}}\right)^{-1/5} \left(\frac{\tilde{E}_{a,k}}{10^{-3}}\right)^{-1/5} \\ &\times \left(\frac{\omega'_a}{\omega_J}\right)^{-2/5} \left(\frac{M}{M_J}\right)^{-2/5} \left(\frac{R}{R_J}\right)^{2/5} \left(\frac{M_*}{M_\odot}\right)^{3/5}, \end{aligned} \quad (32)$$

where $\omega_J^2 \equiv GM_J/R_J^3$. It is interesting to note that $a_{\text{term}}^{(\text{br})}$ has a weak dependence on $\tilde{E}_{a,k}$ ($\simeq \tilde{E}_{\text{resi}}$, since it

⁶ Consistent with the notation in Yu et al. (2021), we use the symbol Δ to specifically indicate the difference between two adjacent orbit.

typically terminates after a wave-breaking event, when the mode energy is small). This is why in Figure 3 the results depend weakly on \tilde{E}_{resi} . The dependence on $\Delta\tilde{E}_1$ is also weak, although it is partially compensated by the fact that $\Delta\tilde{E}_1$ has a very sharp dependence on D_{peri} , scaling as $\Delta\tilde{E}_1 \propto D_{\text{peri}}^{-20}$ (Equations (18) and (20); see also Wu 2018). Consequently, it requires a $\simeq 10\%$ change in D_{peri} in order to change $a_{\text{term}}^{(\text{br})}$ by about 50%. From Figure 2, we see that the change in D_{peri} is much less than 10% for $\tilde{E}_{\text{resi}} = 10^{-3}$. This is why the gray and olive bars at $\Omega/\omega_a = 0$ largely overlap in Figure 3. In other words, the evolution is terminated mostly due to the decrease of a , which reduces both the time P_{orb} for the phase to accumulate and the fractional change $\Delta P_{\text{orb}}/P_{\text{orb}}$ (as the orbit becomes more tightly bound; see also the discussion in Yu et al. 2021). The increase of D_{peri} is a subdominant effect in this case. For greater values of $\tilde{E}_{\text{resi}} = 0.05$, the circularization continues further and D_{peri} could change by a few percent. The increase in D_{peri} now starts to play a role (though still mild) and as a result the final a shown in the cyan bar in Figure 3 is less than a factor of $50^{1/5} \simeq 2$ smaller than the gray one.

For typical propto-HJs, we expect the phase shift to be dominated by the nonlinear frequency shift (Yu et al. 2021). In that case, it is given by ⁷

$$\Delta\phi_{\text{nl},k} \simeq -\omega_a \left(\frac{\Omega}{\omega_a}\right) P_{\text{orb},k} \Delta\tilde{E}_k, \quad (33)$$

where for simplicity we used the leading-order nonlinear frequency shift (Equation (11)) and approximated $\delta\phi_{\text{nl}} \simeq -\Omega\tilde{E}_{a,k}P_{\text{orb},k}$ for each orbit (which applies when $\gamma P_{\text{orb},k} \ll 1$ and $\Gamma\tilde{E}_{a,k}P_{\text{orb},k} \ll 1$). The termination point of a can again be found by setting $|\Delta\phi_{\text{nl},k}| \sim 1$ rad, which gives

$$\begin{aligned} a_{\text{term}}^{(\text{nl})} &\simeq 0.1 \text{ AU} \\ &\times \left(\frac{\lambda_{\text{nl}}}{0.3}\right)^{2/3} \left(\frac{\Delta\tilde{E}_1}{10^{-5}}\right)^{-1/3} \left(\frac{\tilde{E}_{a,k}}{10^{-3}}\right)^{-1/3} \\ &\times \left(\frac{\omega_a}{\omega_J}\right)^{-2/3} \left(\frac{|\Omega/\omega_a|}{30}\right)^{-2/3} \left(\frac{M_*}{M_\odot}\right)^{1/3}, \end{aligned} \quad (34)$$

where we have absorbed the uncertainties in $\Delta\tilde{E}_{a,k}$ and $\Delta\phi_{\text{nl},k}$ together with all the order unity factors into an overall scaling factor λ_{nl} . Note that Equation (34) does

⁷ While this effect originates from nonlinear mode interactions, we note that the phase shift it induces scales with the change in mode energy as $\Delta\phi_{\text{nl},k} \propto \Delta\tilde{E}_{a,k}$. This is the same scaling as the phase shift due to the tidal back-reaction under the linear theory (Equation (31)). Therefore the two effects are formally the same order in $\Delta\tilde{E}_{a,k}$.

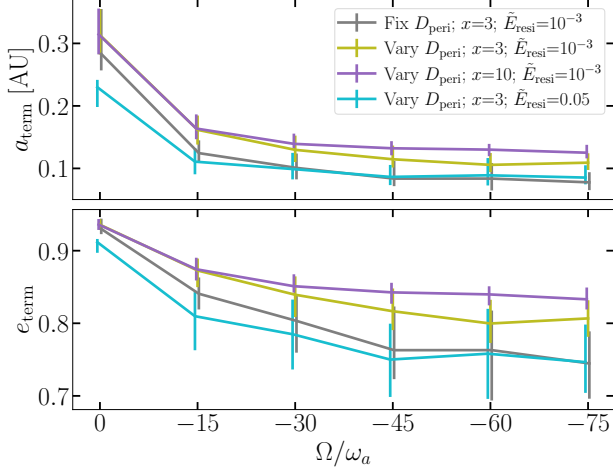


Figure 3. Semi-major axis and eccentricity at which the diffusive tide terminates in the $1.1R_J$ model assuming an orbit with $\Delta\tilde{E}_1 = 1.5 \times 10^{-5}$ and $P_{\text{orb}}^{(f)} = 2.8$ day. The error bars account for differences in the initial conditions (see text). The central point (error bar) corresponds to the median (20 and 80 percentiles) of the resultant distribution. If we ignore the nonlinear phase shift ($\Omega/\omega_a = 0$), $e_{\text{term}} \simeq 0.95$ whereas when we include it $e_{\text{term}} \simeq 0.8$.

not account for the reduction of the nonlinear frequency shift (Equation (26)), which is why in Figure 3 the terminal a decreases slower than $|\Omega/\omega_a|^{-2/3}$.

Comparing Equations (32) and (34), we see that the termination point depends more sensitively on D_{peri} in the nonlinear case. Specifically, $a_{\text{term}}^{(\text{br})} \propto \Delta\tilde{E}_1^{-1/5} \propto D_{\text{peri}}^4$ compared to $a_{\text{term}}^{(\text{nl})} \propto \Delta\tilde{E}_1^{-1/3} \propto D_{\text{peri}}^{6.7}$. For example, a 5% change in D_{peri} can modify $a_{\text{term}}^{(\text{nl})}$ by about 40%. Due to the increase in D_{peri} with time, the circularization stalls at $e \gtrsim 0.7$ even under the most favorable conditions (i.e., small x , large \tilde{E}_{resi} , and large $|\Omega/\omega_a|$).

4.2. The $R = 1.7R_J$ model

We now discuss the results of the $1.7R_J$ model. Notably, its Γ is more than five orders of magnitude larger than that of the $1.1R_J$ model (Table 1). We will see that the f-mode does not undergo wave-breaking as a result.

In Figure 4 we show the evolution of the orbital elements and mode energy assuming representative parameter values. We again assume that the initial orbital semi-major axis is $a_{\text{orb}} = 1$ AU. However, we change the pericenter distance to $D_{\text{peri}} = 0.0315$ AU $\simeq 3.82 r_t$ in order that the one-kick energy $\Delta\tilde{E}_1 = 1.00 \times 10^{-5}$ is again only slightly above the threshold needed to trigger diffusion. The final orbital period in this case is $P_{\text{orb}}^{(f)} = 5.6$ day. Other parameters used to generate the plot are $(x, \tilde{E}_{\text{wb}}, \tilde{E}_{\text{resi}}) = (3, 0.1, 10^{-3})$.

The evolution of $\tilde{E}_{a,k}^{(1)}$ in the $1.7R_J$ model (bottom panel in Figure 4) shows qualitatively different behavior

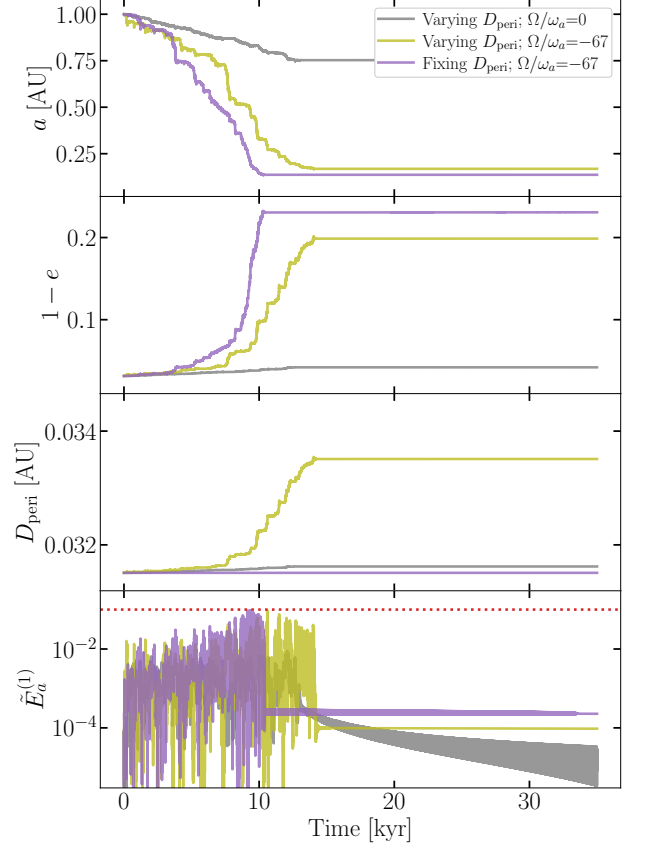


Figure 4. Evolution trajectories of the $1.7R_J$ model. Here we choose a pericenter distance of $D_{\text{peri}} = 0.0315$ AU so that the one-kick energy is $\Delta\tilde{E}_1 = 1.00 \times 10^{-5}$ and the final orbital period is $P_{\text{orb}}^{(f)} = 5.6$ day. Note that during the first 10^4 yr of the evolution, the mode energy is below the wave-breaking limit (red-dotted line in the forth panel) as the dissipation due to turbulent convection and nonlinear interaction is sufficient to balance the energy gain from the orbit.

than in the $1.1R_J$ model. Whereas for the $1.1R_J$ model, $\tilde{E}_{a,k}^{(1)}$ is driven to the wave-breaking value \tilde{E}_{wb} (red-dotted line) in about a hundred years and reaches \tilde{E}_{wb} repeatedly in the subsequent evolution, for the $1.7R_J$ model, it stays below \tilde{E}_{wb} for at least the first 10^4 yr of the evolution when $a \gtrsim 0.2$ AU. This is because the $1.7R_J$ model has a much larger Γ and therefore the nonlinear mode interactions are sufficiently dissipative (Equation (27)) that they can balance the energy gained by the mode at each pericenter passage.

We can estimate the steady-state energy of the mode based on the energy balancing argument

$$2\Gamma\tilde{E}_{a,k}^{(0)}P_{\text{orb}} \simeq \Delta\tilde{E}_{a,k} \sim \sqrt{\tilde{E}_{a,k}^{(0)}\Delta\tilde{E}_1}, \quad (35)$$

where we have used $\tilde{E}_{a,k}^{(1)} \simeq \tilde{E}_{a,k}^{(0)} \gg \Delta\tilde{E}_{a,k} \gg \Delta\tilde{E}_1$ when the mode has built up its energy via the diffusive growth.

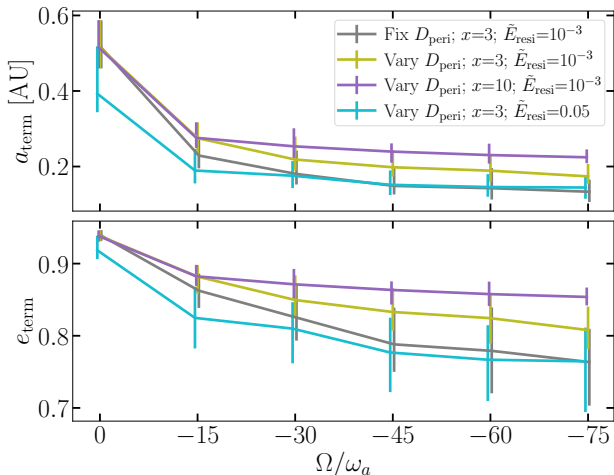


Figure 5. Similar to Figure 3 but for the $1.7R_J$ model with one-kick energy $\Delta\tilde{E}_1 = 10^{-5}$ and final orbital period $P_{\text{orb}}^{(f)} = 5.6$ day.

Dropping factors of order unity, we have

$$\begin{aligned} \tilde{E}_{a,k}^{(0)} &\simeq 10^{-4} \left(\frac{\Delta\tilde{E}_1}{10^{-5}} \right) \left(\frac{\Gamma/\omega_a}{10^{-4}} \right)^{-2} \left(\frac{\omega_a}{\omega_J} \right)^{-2} \\ &\times \left(\frac{M_*}{M_\odot} \right) \left(\frac{a_k}{\text{AU}} \right)^{-3}. \end{aligned} \quad (36)$$

The energy dissipation mechanism is therefore based on a first-principle calculation involving turbulent convection and leading-order nonlinear interactions rather than the ad hoc model of wave breaking used in the $1.1R_J$ case (at least for the first $\sim 10^4$ yr of the evolution). Note, however, that $\tilde{E}_{a,k}^{(0)} \propto a^{-3}$ because as the orbit shrinks, there is less time for the dissipation to take place. As a decays from 1 AU to about 0.2 AU, the steady-state $\tilde{E}_{a,k}^{(0)}$ increases by about a factor of 100, and strongly nonlinear wave-breaking may still eventually occur.

Although the mode now has a qualitatively different evolution trajectory, the orbital elements nonetheless evolve in similar ways for the $1.7R_J$ and $1.1R_J$ models. In particular, the diffusive tide drives significant orbital decay within about 10^4 yr, leading to an effective quality factor (or tidal lag time) similar to the $1.1R_J$ model (see Equation (30)). In addition, the circularization again stalls when the eccentricity is still relatively high ($e \gtrsim 0.8$).

In Figure 5, we examine the statistical properties of the termination point for the $1.7R_J$ model. The conclusions reached for the $1.1R_J$ case (Figure 3) apply again here, including the fact that the terminal eccentricity under the linear theory is $e_{\text{term}} > 0.9$ whereas $e_{\text{term}} \simeq 0.8$ when nonlinear effects are accounted for.

5. SUMMARY AND DISCUSSION

In this work, we revisited the eccentricity distribution of migrating proto-HJs under the influence of the diffusive tide (Section 2). We showed that the diffusive growth of the f-mode results in an especially large tidal lag time (small quality factor; Equations (5) and (30)) that quickly decreases the initially high eccentricity ($e \simeq 1$) to more moderate values ($e \simeq 0.8 - 0.95$). We found that this can explain the observed paucity of super-eccentric proto-HJs with $e > 0.9$ (Dawson et al. 2015), as also found in the linear-theory based diffusive tide study by Wu (2018).

Detecting proto-HJs with $0.8 < e < 0.9$ would more fully test the viability of high-eccentricity migration under the action of the diffusive tide. The recently discovered proto-HJ TOI-3362b by *TESS* (Dong et al. 2021) with $e = 0.815$ is consistent with a planet that has ended the rapid phase of diffusive evolution and entered the slow circularization phase (Equation (5)). The discovery of additional systems like TOI-3362b should help test the diffusive evolution scenario and constrain the termination eccentricity e_{term} .

The system HD 80606b ($e = 0.983$; Wu & Murray 2003) might seem to be an obvious candidate for a proto-HJ undergoing diffusive evolution. However, its radius is too small to trigger diffusion given its pericenter distance (Wu 2018; see also Appendix A). This nonetheless raises an important point regarding the analysis presented in Section 2. Namely, the triggering and termination of the diffusive tide (as captured by Equation (5)) is a complicated function of the orbital and planetary parameters and care must be taken when comparing observations of individual system with the theory.

The phenomenological model in Section 2 was motivated by our analysis of the high-eccentricity evolution of proto-HJs over $\mathcal{O}(10^4)$ yr, which we presented in Sections 3 and 4. This time span is long enough to cover the diffusive tidal evolution from its onset to termination. We extended the treatment of our previous work, Yu et al. (2021), in the following three ways. First, we incorporated into the iterative mapping formalism the evolution of the orbital AM and hence the pericenter distance (Section 3.1). Second, we introduced a phenomenological model (Equation (26)) that prevents unphysically large nonlinear frequency shifts when $|\Omega|\tilde{E}_{a,k} \sim \omega_a$. Lastly, we included weakly nonlinear energy dissipation due to turbulent convective damping and leading-order nonlinear mode interactions, as well as a phenomenological model for strongly nonlinear energy dissipation in the event of wave-breaking of the f-mode (Section 3.3).

With these new ingredients, we examined the coupled mode-orbit evolution for two $M = M_J$ planetary mod-

els, one with radius $1.1R_J$ and the other with radius $1.7R_J$. These were meant to represent an old and young Jupiter, respectively (approximately 10^9 and 10^6 years old). The daughter modes in the $1.1R_J$ model had an especially small turbulent damping rate. Its f-mode therefore grew diffusively until it reached wave-breaking, resulting in episodes of extreme, sudden energy dissipation (Section 4.1). By contrast, the turbulent damping rates of the daughter modes in the $1.7R_J$ model were orders of magnitude larger than in the $1.1R_J$ model. As a result, its f-mode achieved a steady state in which the energy gained at each pericenter passage was balanced by weakly nonlinear dissipation from the excited daughters. We therefore did not need to invoke our phenomenological treatment of wave breaking for the $1.7R_J$ model; the analysis instead relied entirely on first-principle calculations (at least for the first 10^4 yr of the evolution when $a > 0.2$ AU; Section 4.2).

Despite these differences, we found that the two models undergo similar orbital evolution under the diffusive tide. Specifically, the orbital semi-major axis decreases by a factor of a few to ten in $\simeq 10^4$ yr. If we include (neglect) nonlinear mode interactions, the eccentricity decreases from $e \simeq 1$ to $e \simeq 0.8$ ($e \gtrsim 0.9$) before the diffusive growth of the f-mode terminates. Although the impact of nonlinear mode interactions on the termination eccentricity may seem small, we showed in Section 2 that it translates to a significant difference in the number of high- e proto-HJs expected to be found in surveys like *Kepler*.

Although our work can explain the paucity of proto-HJs with $e > 0.9$, our understanding of high-eccentricity tidal migration under the current framework is still far from complete. An especially important issue is the nature of the mechanism that drives the subsequent evolution towards $e \simeq 0$ after the diffusive tide terminates. Even under favorable parameters and assuming the planet can efficiently get rid of the excess AM, we still find significant eccentricities of $e \simeq 0.8$ at termination. In Section 2, we assumed a model with a constant tidal lag time for post-diffusive tidal evolution (as *Socrates et al. 2012* did). *Vick et al. (2019)* showed that the subsequent circularization can be achieved within 10^9 yr if $\tau \gtrsim 1$ s. However, first-principle calculations predict a lag time that is orders of magnitude smaller and closer to $\tau \sim 10^{-8}$ s (*Goldreich & Nicholson 1977*). One possibility is that the damping rate in the planet due to convection is much larger than the original calculations by *Goldreich & Nicholson (1977)* found (see, e.g., *Terquem (2021a,b)*, but also *Barker & Astoul (2021)*). Another possibility is that the planet has highly dissipative g-modes either in the surface layers (*Jermyn et al.*

2017) or in the core (*Mankovich & Fuller 2021*). Alternatively, modes in the host star might become important through either resonant locking (*Ma & Fuller 2021*) or the parametric instability (*Essick & Weinberg 2016*).

A limitation of our current model is that it does not account for the evolution of the planet’s background structure. In order for the orbit to shrink from $a = 1$ AU to 0.1 AU, about $2E_0$ of orbital energy needs to be dissipated. Depositing this amount of energy in the planet could significantly alter its structure (HJs with inflated radii are not necessarily explained by such energy deposition since the planet cools after the diffusive tide terminates; see, e.g., *Baraffe et al. 2010* and references therein). These structural changes may in turn feed back on the diffusive tidal evolution. Meanwhile, if the energy is all dissipated as heat, the mean luminosity of the planet could reach $\sim 5\%L_\odot \sim 10^{-3}L_{\text{Edd}}$, where L_{Edd} is the Eddington luminosity of the planet. This is comparable to the luminosity of a $0.5 M_\odot$ main-sequence star. If the energy dissipates through sudden wave-breaking events, the instantaneous luminosity could even be super-Eddington for brief periods and launch radiation-driven winds (*Wu 2018*).

Another limitation of our analysis is that for simplicity we assume the planet’s rotation rate is constant throughout the diffusive tidal evolution. In effect, we treat the f-mode as a “sink” of orbital AM and do not consider the subsequent transfer of the AM from the f-mode to the background planet, nor the further redistribution of the AM in the planet. Mode-spin coupling and AM transport are challenging problems. In Appendix D, we consider a limiting case where the AM transferred from the orbit to the mode is instantaneously deposited to the background planet and the planet, in turn, instantaneously transports the AM such that it rotates as a solid body throughout the evolution. In this limit, we find that the planet could be spun up significantly, with $\Omega_s > \omega_0$ if it absorbs all the orbital energy and associated orbital AM from $a = 1$ AU to 0.1 AU. In reality, before the planet could ever reach such a high spin rate, the diffusive evolution of the f-mode would likely be quenched. This is because the inertial-frame mode frequency ω'_a then becomes so large that the tidal kick amplitude diminishes significantly (Equation (20)). Such a scenario might be avoided if there is a significant mass outflow that carries away the excess AM. The orbital decay timescale under the diffusive tide would then likely be limited by the spin-down timescale. Alternatively, planetary inertial modes could be excited if the planet rotates near the critical spin rate (*Papaloizou & Ivanov 2005; Ivanov & Papaloizou 2007; Xu & Lai 2017; Vick et al. 2019*), which may allow the diffusive tidal

evolution to persist. Understanding the spin evolution of the planet during diffusive growth is an important topic that future studies will need to address.

We thank Fei Dai for helpful discussions and comments during the preparation of the manuscript. This work was supported by NSF AST-2054353. H.Y. acknowledges the support of the Sherman Fairchild Foundation.

APPENDIX

A. DIFFUSIVE GROWTH THRESHOLD AS A FUNCTION OF FINAL ORBITAL PERIOD AND PLANETARY RADIUS

In the analysis presented in Section 2, we grouped systems only according to their final orbital period $P_{\text{orb}}^{(f)}$. While such a simple grouping is consistent with the analysis performed by [Socrates et al. \(2012\)](#) and is typically done observationally (e.g., [Dawson et al. 2015](#)), we point out here as a caveat that it may oversimplify the problem.

For example, the number density can also be a sensitive function of the planetary radius R . In part, this is because R would enter the overall timescale $T(e)$ as R^{-5} (Equation 4). More importantly, the tidal lag time τ in Equation (5) should be treated as a function of R as well, because the threshold for diffusive growth to happen is sensitive to R .

We explore this point in detail in Figure 6. Here we show the maximum $P_{\text{orb}}^{(f)}$ at which diffusive growth can happen as a function of R . Our calculation follows section 5.1 in [Yu et al. \(2021\)](#). To generate the curves, we fix $(M, M_*) = (M_J, M_\odot)$ and $a = 1$ AU. We further set $\omega_a = 1.1\omega_0$ and $Q_a = 0.4$. The planet is assumed to be non-rotating; including rotation would reduce the maximum $P_{\text{orb}}^{(f)}$ allowed further as it reduces the tidal kick at the pericenter.

One might argue that the diffusive tide is a necessary component for the high-eccentricity tidal migration of proto-HJs. This is because it simultaneously makes the overall circularization timescale shorter than the age of the host star and it prevents the eccentricity from getting excited to too high a value, thereby saving the planet from being disrupted by the host star (see, e.g., the discussion in [Vick et al. 2019](#)). If this is the case, then Figure 6 suggests that the final orbital period of an HJ would be highly correlated with its initial radius, as only Jupiters with $R \gtrsim 1.5R_J$ could successfully migrate to an orbit with $P_{\text{orb}}^{(f)} = 5$ day. However, this correlation may be washed out for HJs today because after undergoing diffusive evolution, the planet has sufficient time to cool and contract (and possibly re-inflate), making their current radii differ from their initial ones.

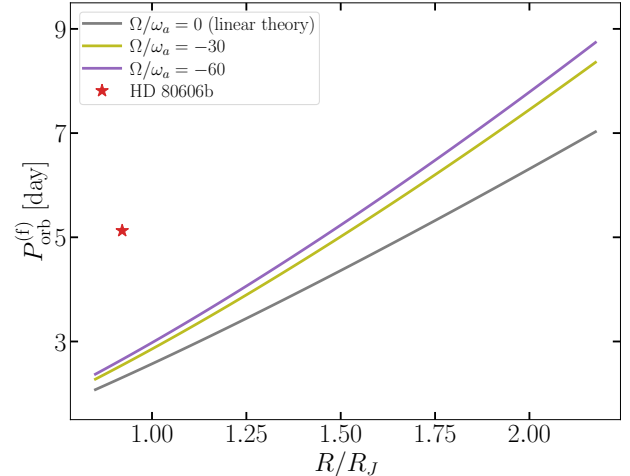


Figure 6. Maximum $P_{\text{orb}}^{(f)}$ at which the diffusive tide can still be triggered as a function of the planetary radius. The gray line corresponds to the threshold calculated under the linear theory, while the olive and purple lines include the phase shift induced by nonlinear mode interactions assuming different values of Ω/ω_a (Table 1). The system HD 80606b (red star) is above the threshold and therefore will not undergo diffusive growth.

Figure 6 further suggests that to make accurate predictions of the eccentricity distribution, more careful studies that include population synthesis and planetary evolution are necessary.

B. TIDAL ANGULAR MOMENTUM TRANSFER

In this appendix, we calculate the amount of AM transferred from the orbit to the modes as a function of the energy transferred to the modes. The energy deposited from the orbit to the planet is

$$\begin{aligned} \dot{E}(t) &= - \int d^3x \rho \dot{\xi} \cdot \nabla U \\ &= \sum_a (i\omega_a) q_a^*(t) U_a(t) E_0, \\ &= -2 \sum_{\omega_a > 0} \text{Im} [\omega_a q_a^* U_a] E_0, \end{aligned} \quad (\text{B1})$$

where in the second line we have used the modal expansion to expand the velocity $\dot{\xi}$ into eigenmodes.

The torque \mathcal{T} acting on the planet can be derived from an interaction Hamiltonian (see, e.g., Yu et al. 2020),

$$H_{\text{int}} = \sum_{\omega_a > 0} [q_a U_a^* + q_a^* U_a] E_0, \quad (\text{B2})$$

leading to

$$\begin{aligned} \mathcal{T} &= \frac{\partial H_{\text{int}}}{\partial \Phi} = -2 \sum_{\omega_a > 0} \text{Re} \left[q_a^* \frac{\partial U_a}{\partial \Phi} \right] E_0, \\ &= -2 \sum_{\omega_a > 0} \text{Im} [m_a q_a^* U_a] E_0. \end{aligned} \quad (\text{B3})$$

Thus the energy transfer to a mode ΔE_a is related to the AM transfer to the mode ΔJ_a by

$$\Delta E_a = \frac{\omega_a}{m_a} \Delta J_a. \quad (\text{B4})$$

The same relation can also be derived from the Lagrangian of the perturbed fluid. See, e.g., Friedman & Schutz (1978) for details.

It is also interesting to consider how the energy/AM transfer affects the orbit (see Equation (23)). This can be done by dividing both sides of Equation (B4) by $|E_{\text{orb}}| = \Omega_{\text{orb}} L/2$, leading to

$$\frac{\Delta E_a}{|E_{\text{orb}}|} = \frac{2\omega_a}{m_a \Omega_{\text{orb}}} \frac{\Delta J_a}{L}. \quad (\text{B5})$$

Therefore, for a highly eccentric orbit with $\omega_a (\gtrsim \Omega_{\text{peri}}) \gg \Omega_{\text{orb}}$, the fractional change in the orbital AM L is much smaller than the fractional change in the orbital energy E_{orb} .

C. PROPERTIES OF THE $1.7R_J$ JUPITER MODEL

We show here the properties of the daughter modes in the $1.7R_J$ model. The calculations closely follow those of section 3.3 in Yu et al. (2021).

In Figure 7, we show the linear frequency, the coupling coefficient with the parent mode (Weinberg et al. 2012), and the linear damping rate due to turbulent convection of each daughter mode (Shiode et al. 2012; Burkart et al. 2013).

From the linear properties of the daughter modes, we can compute their contributions to the nonlinear frequency shift Ω and damping rate Γ following Yu et al. (2021). The result is shown in Figure 8. Here in the colored curves, we show each mode's contribution, with a “+(-)” symbol indicating a positive (negative) value. In the gray curves, we plot the cumulative contributions to Ω and Γ from modes with radial order $\geq n_a$ and all values of (l_a, m_a) allowed by the angular selection rules (Weinberg et al. 2012).

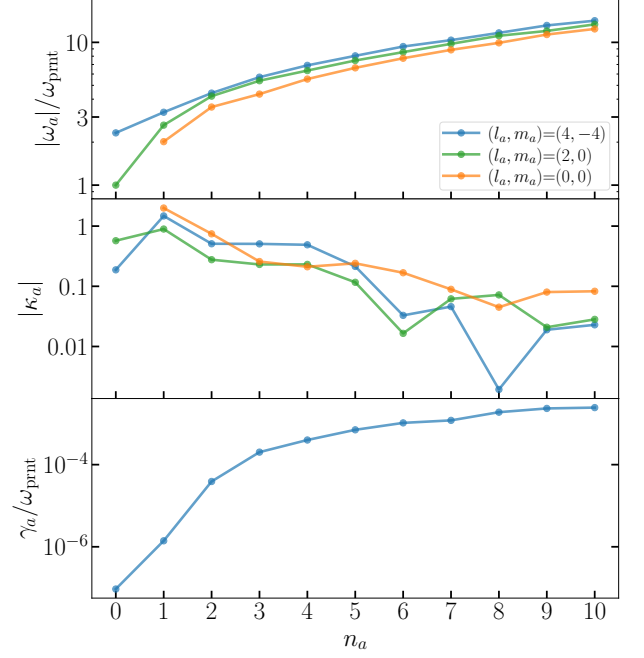


Figure 7. Eigenfrequency, coupling coefficient, and linear damping rate of modes of the $R = 1.7R_J$ model as a function of their radial order n_a (see key in the top panel for their l_a and m_a). Here we use the subscript “ a ” to stand for a generic mode, and we use ω_{pnt} to indicate specifically the linear eigenfrequency of the parent (i.e., the frequency given in Table 1).

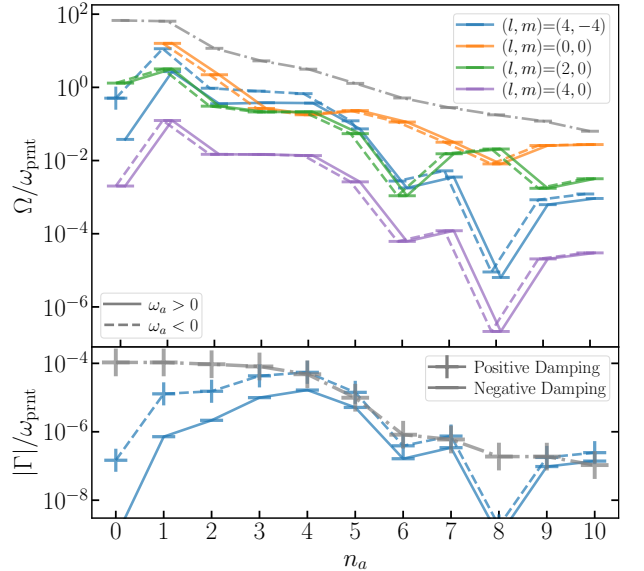


Figure 8. Each linear eigenmode’s contribution to the nonlinear frequency shift parameter Ω (top) and dissipation rate parameter Γ (bottom).

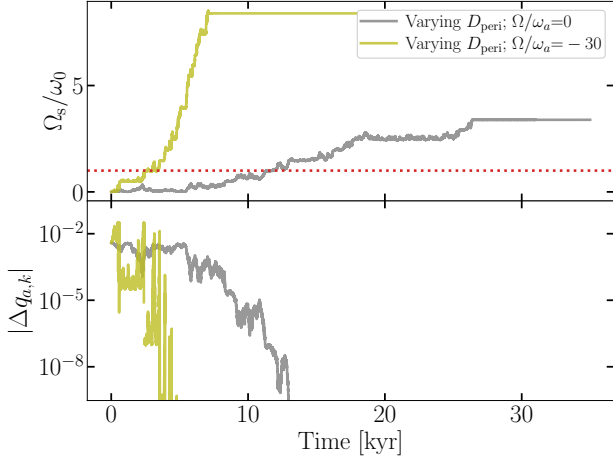


Figure 9. Spin evolution (top panel) and the kick amplitude (bottom panel) found by post-processing the trajectories shown in Figure 2.

D. SPIN AS AN ALTERNATIVE CHANNEL FOR TERMINATING DIFFUSIVE GROWTH

In the main text, we assumed that the f-mode acts as the ultimate sink of the AM. Here we consider the possibility that the orbital AM transferred into the f-mode then gets deposited in the background planet and spins it up. For simplicity, we assume that the transfer from the mode to the planet is instantaneous and that the planet maintains a solid-body rotation at all times. Under these assumptions, we show that the spin-up of the background planet can be another process by which the diffusive growth terminates.

In Figure 9 we show the spin evolution $\Omega_s(t)$ found by *post-processing* the trajectories in Figure 2. In other words, we use the ΔJ_a computed when generating Figure 2 to calculate the spin rate of the planet at the k 'th orbit according to $\Omega_{s,k} = \sum_i^k \Delta J_{a,i} / I$, where $I = 0.38MR^2$ is the moment of inertia of the $1.1R_J$ model. Once we have the spin of the background planet, we can also calculate the kick amplitude at each pericenter passage according to Equation (20) with the new $\omega'_{a,k} = \omega_a + m_a \Omega_{s,k}$. The result is shown in the lower panel in Figure 9. Note, however, that since this is done in post-processing we do not further change the evolution trajectories based on the new $\Delta q_{a,k}$.

The top panel shows that the planet spins-up significantly. This is because in order for the orbit to shrink from $a \simeq 1$ AU to $\simeq 0.1$ AU, the total amount of energy that needs to be transferred into the planet and dissipated can be few times E_0 . From Equation (B4), the total amount of orbital AM absorbed is

$$\frac{\Delta J_a}{J_0} = \left(\frac{m_a \omega_0}{\omega_a} \right) \left(\frac{\Delta E_a}{E_0} \right), \quad (\text{D6})$$

where $J_0 \equiv \omega_0 MR^2$.

In fact, before the planet reaches such a large spin rate, the diffusive evolution is likely to terminate because of the sharp decrease of $|\Delta q_{a,k}|$ with increasing ω'_a , as indicated in the bottom panel (see also Equation (20)). If the AM gained by the background planet cannot be removed somehow, this would limit the total amount of orbital energy decay to be $\ll E_0$. One potential way to prevent such a large spin-up and thereby delay the termination of the diffusive evolution is if the planet drives a wind that induces a strong spin-down torque (e.g. a magnetic Weber-Davis wind; Weber & Davis 1967). For moment-arm R_A , the AM loss rate scales as

$$j = \frac{2}{3} \dot{M} \Omega_s R_A^2, \quad (\text{D7})$$

where \dot{M} is the mass loss rate. We can thus define a spin-down timescale τ_{sd} as the time for the wind to remove J_0 from the planetary AM,

$$\begin{aligned} \tau_{\text{sd}} &= \frac{J_0}{j} = \frac{3}{2} \left(\frac{M}{\dot{M}} \right) \left(\frac{R}{R_A} \right)^2 \left(\frac{\omega_0}{\Omega_s} \right), \\ &\simeq 2 \times 10^4 \text{yr} \left(\frac{\dot{M}/M}{10^{-5} \text{yr}^{-1}} \right)^{-1} \left(\frac{R_A/R}{3} \right)^{-2} \left(\frac{\omega_0}{\Omega_s} \right) \end{aligned} \quad (\text{D8})$$

where the co-rotating moment arm (determined by, e.g., the magnetosphere) has been assumed to extend to $R_A = 3R$. In other words, the planet needs to have a significant mass loss rate of $\dot{M}/M \sim 10^{-5} \text{yr}^{-1}$ in order to keep the spin rate low enough that the diffusive evolution can continue unabated.

In the absence of such a powerful outflow, the circularization timescale will be limited by the spin-down timescale, if in fact there is any significant spin-down mechanism. In this case, the diffusive tide could only operate momentarily before it is shut down by the rapid spin of the planet. We would then need to wait for the mass outflow to slowly remove the AM until $|\Delta q_{a,k}|$ becomes large to be able to trigger diffusion again. The time to circularize the orbit can then be no faster than the spin-down timescale τ_{sd} .

Regardless of the mass loss rate, the total amount of mass that needs to be removed is given by

$$\frac{\Delta M}{M} = \frac{3}{2} \left(\frac{\Delta J_a}{J_0} \right) \left(\frac{R}{R_A} \right)^2 \left(\frac{\omega_0}{\Omega_s} \right). \quad (\text{D9})$$

Therefore, a significant amount of mass and angular momentum loss is likely required in order for the f-mode to experience a significant diffusive growth.

REFERENCES

- Baraffe, I., Chabrier, G., & Barman, T. 2010, *Reports on Progress in Physics*, 73, 016901, doi: [10.1088/0034-4885/73/1/016901](https://doi.org/10.1088/0034-4885/73/1/016901)
- Barker, A. J., & Astoul, A. A. V. 2021, *MNRAS*, 506, L69, doi: [10.1093/mnrasl/slab077](https://doi.org/10.1093/mnrasl/slab077)
- Burkart, J., Quataert, E., Arras, P., & Weinberg, N. N. 2013, *MNRAS*, 433, 332, doi: [10.1093/mnras/stt726](https://doi.org/10.1093/mnras/stt726)
- Burke, C. J., Bryson, S. T., Mullally, F., et al. 2014, *ApJS*, 210, 19, doi: [10.1088/0067-0049/210/2/19](https://doi.org/10.1088/0067-0049/210/2/19)
- Chatterjee, S., Ford, E. B., Matsumura, S., & Rasio, F. A. 2008, *ApJ*, 686, 580, doi: [10.1086/590227](https://doi.org/10.1086/590227)
- Darwin, G. H. 1879, *Philosophical Transactions of the Royal Society of London Series I*, 170, 1
- Dawson, R. I., Murray-Clay, R. A., & Johnson, J. A. 2015, *ApJ*, 798, 66, doi: [10.1088/0004-637X/798/2/66](https://doi.org/10.1088/0004-637X/798/2/66)
- Dong, J., Huang, C. X., Zhou, G., et al. 2021, *ApJL*, 920, L16, doi: [10.3847/2041-8213/ac2600](https://doi.org/10.3847/2041-8213/ac2600)
- Essick, R., & Weinberg, N. N. 2016, *ApJ*, 816, 18, doi: [10.3847/0004-637X/816/1/18](https://doi.org/10.3847/0004-637X/816/1/18)
- Fabrycky, D., & Tremaine, S. 2007, *ApJ*, 669, 1298, doi: [10.1086/521702](https://doi.org/10.1086/521702)
- Friedman, J. L., & Schutz, B. F. 1978, *ApJ*, 221, 937, doi: [10.1086/156098](https://doi.org/10.1086/156098)
- Goldreich, P., Murray, N., Longaretti, P. Y., & Banfield, D. 1989, *Science*, 245, 500, doi: [10.1126/science.245.4917.500](https://doi.org/10.1126/science.245.4917.500)
- Goldreich, P., & Nicholson, P. D. 1977, *Icarus*, 30, 301, doi: [10.1016/0019-1035\(77\)90163-4](https://doi.org/10.1016/0019-1035(77)90163-4)
- Goldreich, P., & Soter, S. 1966, *Icarus*, 5, 375, doi: [10.1016/0019-1035\(66\)90051-0](https://doi.org/10.1016/0019-1035(66)90051-0)
- Hamers, A. S., Antonini, F., Lithwick, Y., Perets, H. B., & Portegies Zwart, S. F. 2017, *MNRAS*, 464, 688, doi: [10.1093/mnras/stw2370](https://doi.org/10.1093/mnras/stw2370)
- Hut, P. 1981, *A&A*, 99, 126
- Ivanov, P. B., & Papaloizou, J. C. B. 2004, *MNRAS*, 347, 437, doi: [10.1111/j.1365-2966.2004.07238.x](https://doi.org/10.1111/j.1365-2966.2004.07238.x)
- . 2007, *MNRAS*, 376, 682, doi: [10.1111/j.1365-2966.2007.11463.x](https://doi.org/10.1111/j.1365-2966.2007.11463.x)
- Jermyn, A. S., Tout, C. A., & Ogilvie, G. I. 2017, *MNRAS*, 469, 1768, doi: [10.1093/mnras/stx831](https://doi.org/10.1093/mnras/stx831)
- Lai, D. 1997, *ApJ*, 490, 847, doi: [10.1086/304899](https://doi.org/10.1086/304899)
- Ma, L., & Fuller, J. 2021, arXiv e-prints, arXiv:2105.09335. <https://arxiv.org/abs/2105.09335>
- Mankovich, C., & Fuller, J. 2021, arXiv e-prints, arXiv:2104.13385. <https://arxiv.org/abs/2104.13385>
- Mardling, R. A. 1995, *ApJ*, 450, 722, doi: [10.1086/176178](https://doi.org/10.1086/176178)
- Muñoz, D. J., Lai, D., & Liu, B. 2016, *MNRAS*, 460, 1086, doi: [10.1093/mnras/stw983](https://doi.org/10.1093/mnras/stw983)
- Ogilvie, G. I. 2014, *ARA&A*, 52, 171, doi: [10.1146/annurev-astro-081913-035941](https://doi.org/10.1146/annurev-astro-081913-035941)
- Ogilvie, G. I., & Lin, D. N. C. 2004, *ApJ*, 610, 477, doi: [10.1086/421454](https://doi.org/10.1086/421454)
- Papaloizou, J. C. B., & Ivanov, P. B. 2005, *MNRAS*, 364, L66, doi: [10.1111/j.1745-3933.2005.00107.x](https://doi.org/10.1111/j.1745-3933.2005.00107.x)
- Paxton, B., Bildsten, L., Dotter, A., et al. 2011, *ApJS*, 192, 3, doi: [10.1088/0067-0049/192/1/3](https://doi.org/10.1088/0067-0049/192/1/3)
- Paxton, B., Cantiello, M., Arras, P., et al. 2013, *ApJS*, 208, 4, doi: [10.1088/0067-0049/208/1/4](https://doi.org/10.1088/0067-0049/208/1/4)
- Paxton, B., Marchant, P., Schwab, J., et al. 2015, *ApJS*, 220, 15, doi: [10.1088/0067-0049/220/1/15](https://doi.org/10.1088/0067-0049/220/1/15)
- Paxton, B., Schwab, J., Bauer, E. B., et al. 2018, *ApJS*, 234, 34, doi: [10.3847/1538-4365/aaa5a8](https://doi.org/10.3847/1538-4365/aaa5a8)
- Paxton, B., Smolec, R., Schwab, J., et al. 2019, *ApJS*, 243, 10, doi: [10.3847/1538-4365/ab2241](https://doi.org/10.3847/1538-4365/ab2241)
- Petrovich, C., & Tremaine, S. 2016, *ApJ*, 829, 132, doi: [10.3847/0004-637X/829/2/132](https://doi.org/10.3847/0004-637X/829/2/132)
- Press, W. H., & Teukolsky, S. A. 1977, *ApJ*, 213, 183, doi: [10.1086/155143](https://doi.org/10.1086/155143)
- Rasio, F. A., & Ford, E. B. 1996, *Science*, 274, 954, doi: [10.1126/science.274.5289.954](https://doi.org/10.1126/science.274.5289.954)
- Schenk, A. K., Arras, P., Flanagan, É. É., Teukolsky, S. A., & Wasserman, I. 2002, *PhRvD*, 65, 024001, doi: [10.1103/PhysRevD.65.024001](https://doi.org/10.1103/PhysRevD.65.024001)
- Shiode, J. H., Quataert, E., & Arras, P. 2012, *MNRAS*, 423, 3397, doi: [10.1111/j.1365-2966.2012.21130.x](https://doi.org/10.1111/j.1365-2966.2012.21130.x)
- Socrates, A., Katz, B., Dong, S., & Tremaine, S. 2012, *ApJ*, 750, 106, doi: [10.1088/0004-637X/750/2/106](https://doi.org/10.1088/0004-637X/750/2/106)
- Terquem, C. 2021a, *MNRAS*, 503, 5789, doi: [10.1093/mnras/stab224](https://doi.org/10.1093/mnras/stab224)
- . 2021b, arXiv e-prints, arXiv:2106.15547. <https://arxiv.org/abs/2106.15547>
- Teyssandier, J., Naoz, S., Lizarraga, I., & Rasio, F. A. 2013, *ApJ*, 779, 166, doi: [10.1088/0004-637X/779/2/166](https://doi.org/10.1088/0004-637X/779/2/166)
- Townsend, R. H. D., Goldstein, J., & Zweibel, E. G. 2018, *MNRAS*, 475, 879, doi: [10.1093/mnras/stx3142](https://doi.org/10.1093/mnras/stx3142)
- Townsend, R. H. D., & Teitler, S. A. 2013, *MNRAS*, 435, 3406, doi: [10.1093/mnras/stt1533](https://doi.org/10.1093/mnras/stt1533)
- Vick, M., & Lai, D. 2018, *MNRAS*, 476, 482, doi: [10.1093/mnras/sty225](https://doi.org/10.1093/mnras/sty225)
- Vick, M., Lai, D., & Anderson, K. R. 2019, *MNRAS*, 484, 5645, doi: [10.1093/mnras/stz354](https://doi.org/10.1093/mnras/stz354)
- Weber, E. J., & Davis, Leverett, J. 1967, *ApJ*, 148, 217, doi: [10.1086/149138](https://doi.org/10.1086/149138)
- Weinberg, N. N., Arras, P., Quataert, E., & Burkart, J. 2012, *ApJ*, 751, 136, doi: [10.1088/0004-637X/751/2/136](https://doi.org/10.1088/0004-637X/751/2/136)
- Wu, Y. 2018, *AJ*, 155, 118, doi: [10.3847/1538-3881/aaa970](https://doi.org/10.3847/1538-3881/aaa970)
- Wu, Y., & Lithwick, Y. 2011, *ApJ*, 735, 109, doi: [10.1088/0004-637X/735/2/109](https://doi.org/10.1088/0004-637X/735/2/109)

Wu, Y., & Murray, N. 2003, *ApJ*, 589, 605,
doi: [10.1086/374598](https://doi.org/10.1086/374598)

Xu, W., & Lai, D. 2017, *PhRvD*, 96, 083005,
doi: [10.1103/PhysRevD.96.083005](https://doi.org/10.1103/PhysRevD.96.083005)

Yu, H., Weinberg, N. N., & Arras, P. 2021, *ApJ*, 917, 31,
doi: [10.3847/1538-4357/ac0a79](https://doi.org/10.3847/1538-4357/ac0a79)

Yu, H., Weinberg, N. N., & Fuller, J. 2020, *MNRAS*, 496,
5482, doi: [10.1093/mnras/staa1858](https://doi.org/10.1093/mnras/staa1858)